Lenis, J.; Bejarano, G.; Rico Tortosa, PM.; Gómez Ribelles, JL.; Bolívar, F. (2019). Development of multilayer Hydroxyapatite - Ag/TiN-Ti coatings deposited by radio frequency magnetron sputtering with potential application in the biomedical field. Surface and Coatings Technology. 377:1-9. https://doi.org/10.1016/j.surfcoat.2019.06.097

Development of multilayer Hydroxyapatite- Ag/TiN-Ti coatings deposited by radio frequency magnetron sputtering with potential application in the biomedical field

*J.A. Lenis *[a], G. Bejarano [a], P. Rico [b,c], J.L Gómez Ribelles [b,c], F.J. Bolívar [a].*

[a] Centro de Investigación, innovación y Desarrollo de Materiales CIDEMAT, Facultad de ingeniería, Universidad de Antioquia, Medellín, Colombia.

[b] Centre for Biomaterials and Tissue Engineering, CBIT, Universitat Politècnica de València, Spain.

[c] Biomedical Research Networking Center in Bioengineering, Biomaterials and Nanomedicine (CIBER-BBN), Valencia, Spain.

Abstract

The use of composite coatings is emerging as a great alternative to conventional coatings, allowing the combination of different superficial properties that are widely desired in surgical implants, such as osteointegration and bactericidal character, and cannot be provided by one material alone. In the present investigation the effect of the incorporation of a TiN-Ti intermediate bilayer on the chemical composition, structure, morphology, roughness, residual stresses and adhesion of a multi-layer Hydroxyapatite (HA)-Ag coating deposited on Ti-6Al-4V by magnetron sputtering was evaluated. Additionally, the cytotoxicity of the developed system was evaluated by *in vitro* tests. According to the results obtained, a decrease in the Ca/P ratio from 1.85 to 1.74 was obtained through the deposition of an HA-Ag system on the intermediate bilayer, and the crystallinity of the developed coating was favored. The multi-layer structure was effectively observed by field emission scanning electron microscopy, where it was possible to identify each of the HA, Ag, TiN and Ti layers. Meanwhile, an increase of 7% in crystallite size, a decrease of 36% in residual stresses and an increase of 32% in adhesion were registered for this composite coating compared

to the free intermediate bilayer system. Finally, biological evaluation allowed the non-cytotoxic character of the deposited coatings to be confirmed.

Keywords: Magnetron sputtering, Hydroxyapatite, Ca/P ratio, Structure, Multi-layer coating, Intermediate layers, Critical load, Cytotoxicity.

1. Introducción

Hydroxyapatite (HA) is a calcium phosphate with the molecular formula $Ca_5(PO_4)_3OH$, which has a high osteointegration due to its chemical similarity with bone mineral. For this reason it has been widely used as a component for implant manufacture [1,2]. Its mechanical resistance is low, so it is normally used for filling small cavities or prosthetic replacement in zones subject to low loads [3,4]. Nevertheless, for some years it has been used to coat metal surfaces which provide greater mechanical support, which extends its range of applications in the biomedical field [5,6]. Among the techniques commonly used to obtain HA coatings, magnetron sputtering (MS) has been found to give these films high homogeneity, compaction and purity. In addition, the highest adhesion values between this biomaterial and, for example, the Ti-6Al-4V alloy, have been obtained by this technique [7]. Through surface modification of this alloy by deposition of an HA coating, it is possible to induce osteointegration and to promote the coating's corrosion resistance, since these films usually act as a barrier layer and prevent the possible migration of Al^{3+} and V^{2+} ions to the medium, which can generate long-term cytotoxicity [8]. Additionally, the use of intermediate transition layers between the HA and the metallic substrate can widely favor all these properties [9]. E. Mohseni *et al.* [4] deposited a TiN intermediate layer in order to improve adhesion in an HA / Ti-6Al-4V system. TiN is also biocompatible, besides having high chemical stability and wear resistance, making it optimal for this type of application [10]. Regarding the development of

this coatings by MS, the effect of doping HA with different elements has been studied in order to enhance its properties in general. E.S. Thian *et al.* [11] improved cell proliferation and calcification in HA coatings doped with Si. Additionally, an enhancement in the mechanical properties of HA coatings has been reported by A. Vladescu *et al.* [12] through SiC incorporation. The inclusion of this last element favored corrosion resistance and bioactivity in HA coatings [13]. Furthermore, different doping elements are currently being evaluated in order to induce antibacterial properties in HA coatings and thus protecting its surface against possible bacterial colonization, without affecting biocompatibility. Silver (Ag) is quite an attractive element for this purpose since it has a broad antibacterial spectrum, acting effectively against both gram-positive and gram-negative strains [14]. A. Peetsch *et al.* [15] evaluated antibacterial properties and cytotoxicity in CaP nanoparticles doped with Ag, with results that showed minimum bactericidal concentrations of 0.62 and 1.25 µg Ag/mL for *Escherichia coli* and *Staphylococcus aureus*, respectively. Nevertheless, for human mesenchymal stem cells and peripheral blood mononuclear cells, toxic effects above 2.5 µg Ag/mL were found. The combination of both bactericidal and osteointegration properties in HA-Ag composite coatings makes them attractive for potential use in the biomedical field. However, currently there are very few reports about the incorporation of intermediate layers between this system and metallic substrates, and none on the influence of these interlayers on the microstructure and other properties of HA. In the present work, a multilayer HA-Ag/TiN-Ti coating was deposited on a Ti-6Al-4V alloy; the effect of the incorporation of the intermediate bilayer on the chemical composition, structure, phases, mechanical properties and cytotoxicity of the HA-Ag coating was studied by means of spectroscopic, microscopic, X-ray diffraction, and nano-indentation techniques; and the cell viability was evaluated using murine embryonic mesenchymal stem cells C3H10T1/2 (mMSCs).

2. Materials and methods

2.1. Obtaining coatings

Ti-6Al-4V samples of 10×10×3 mm^3 were used as substrates. Surface preparation of these was performed by mechanical polishing until a mirror-like finish was obtained. In order to eliminate impurities and organic contaminants, these samples were immersed in a 3:1 ethanol-acetone solution and placed in an ultrasonic bath (60 Hz, Intertek CD-4800) for 15 min. The Ti-6Al-4V surface was then cleaned by argon sputtering (1 keV, 15 min) before starting the deposition process. This was performed in a rectangular MS device (with dimensions of 700×700×800 mm^3, equipped with a radio frequency (RF) source (13.46 MHz, SEREM), and direct current (DC) source (ADL, MARIS). To obtain the coatings, 3 targets were used: Ti (99.95% purity), HA (99.99% purity) and Ag (99.9% purity), with dimensions of 500×100×6 mm^3 each. Initially, a coating of TiN-Ti was obtained, deposited at a power of 1.2 kW DC, temperature of 250°C, pressure of 0.5 Pa and applying a bias voltage of -70 V to the substrates. These conditions were selected taking into account previous work done in the research group [16,17]. For the initial Ti layer, the deposition process was carried out with argon (99.9% purity), for 10 min, while to obtain the TiN layer a reactive atmosphere was used with a 2:1 argon-nitrogen mixture. The HA-Ag multi-layer coating was deposited applying a power of 600 W RF to the HA target and 20 W DC to the Ag target. The process was carried out at 200°C, 0.5 Pa and applying a bias voltage of - 20V to the substrates. The architecture of the coatings developed consisted of 5 HA layers with 4 intermediate Ag layers, obtained by rotating the sample holder for the deposition of each of the elements. The HA deposition time was 300 min, which was selected based on a previous report [18], while the Ag deposition time was 12 min. Fig. 1 shows the schematic configuration of the system developed.

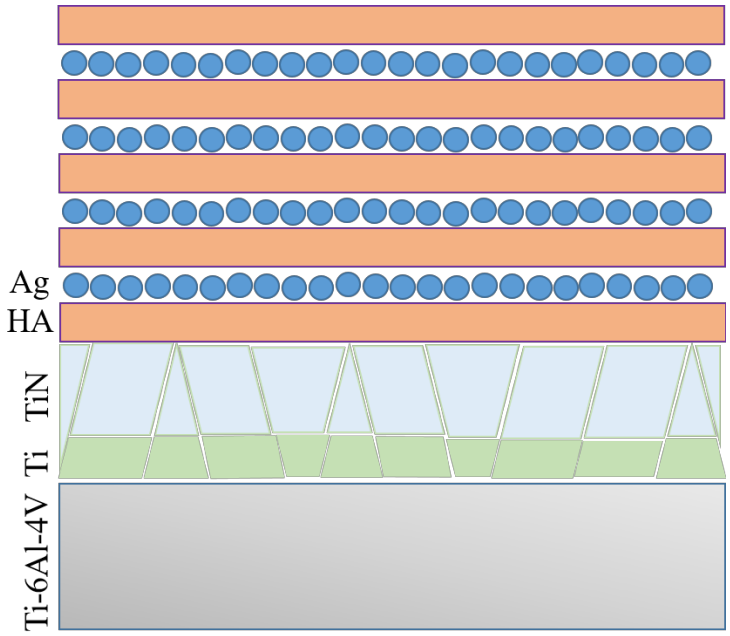

Figure 1. Schematic architecture of the developed multi-layer coating

2.2. Chemical composition, phases and crystallinity

Elemental composition analysis was performed in triplicate over an area of 35×35 μm^2 by energy dispersive spectroscopy (EDS) using a Jeol instrument (JSM-6490LVTM, 20 kV). Micro-Raman spectroscopy was used in order to identify the characteristic vibration of the functional groups present in the coatings between 200 cm^{-1} and 1200 cm^{-1}; for which irradiation was performed with a He-Ne laser of 633 nm and power of 17 mW using a Horiba Jobinyvon, Model Labram HR instrument. The crystallinity of the coatings was evaluated in a range of 16° to 34° 2Θ, at 0.7°/min, using an X-ray diffractometer (Panlitycal X'pert pro MPD) with Cukα radiation λ=1.540598 Å, 45 kV, 40 mA. Also, the crystallite size for the HA-Ag coatings was determined using the Scherrer equation [19] (equation 1), for which the Full Width at Half Maximum (FWHM) of the diffraction peaks was calculated using a Gaussian adjustment with the W'pert high software.

$$\beta = \frac{(k).(\lambda)}{(FWHM).(COS\ \theta)} \quad (1)$$

Where β is the crystallite size, k is the crystal shape factor, λ is the wavelength of the radiation used and Θ is the measured angle.

2.3. Structure, morphology, roughness and wettability

In the first instance, the structure of the coatings in cross-section was appreciated by scanning electron microscopy (SEM) (Jeol instrument JSM-6490LVTM, 20 kV). However, with this technique it was not possible to clearly observe the HA-Ag multi-layers. For this reason, a cut of 5×5×2 μm^3 was made on the surface of the coatings using focused ion beam (FIB) (ZEISS AURIGA Compact dual beam system at 30 kV, 500 pA), and subsequently the structure was observed by field emission scanning electron microscopy (FESEM) using the same equipment at 2 kV, 50 pA. Additionally, the morphology of the coatings was evaluated at 8,000X magnification. The roughness of the coatings was measured in triplicate over an area of 5×5 μm^2 by atomic force microscopy (MFP-3D Infinity, Oxford Instruments Asylum) operated in AC Mode. The nominal spring constant was 2.5 N/m and the resonance frequency was 73.52 kHz. Meanwhile, the wettability of the surfaces was determined with a water drop of 3 μL using a goniometer (Ramé-Hast) and the surface free energy was calculated by the Neumann method [20], which is based on equation 2:

$$\cos\theta = 2\left(\frac{\gamma s}{\gamma L}\right)^{0.5} \exp\left[-\beta(\gamma L - \gamma s)^2\right] - 1 \quad (2)$$

Where γS is the coating surface free energy, γL = 72.8 mJ / m^2, β = 0.0001247 m^2 / mJ and Θ is the water contact angle.

2.4. Mechanical evaluation

N-type Silicon samples of 20×3×0.5 mm^3, with preferential orientation along (100) plane were coated with HA-Ag and HA-Ag/TiN-Ti coatings, and the change in the coatings' curvature radius was measured in order to calculate the residual stresses generated during the films' formation by using the Stoney equation [21]. For this, a Bruker DektakXT model profiler equipped with a silicon tip was used. The distance evaluated in each sample was 25 mm and the measurements were made in triplicate. The adhesion of the systems was evaluated by micro-scratch tests, using a nano-indentation system (MTS's XP System Corporation) equipped with a conical diamond tip (Rockwell C) with 10 μm in diameter. The scratch distance was fixed at 2000 μm and a progressive load up to 350 mN was applied at a speed of 3.21 mN/s on the coatings' surface.

2.5. Cytotoxicity tests

Cell viability test carried out by the LIVE/DEAD™ assay. In this, distinctive characteristics of living cells were determined by means of the intracellular esterase activity using calcein AM staining, which generated a fluorescent green color, while for dead cells, the loss of the integrity of the plasma membrane was observed by staining with ethidium homodimer-1, generating a fluorescent red color. mMSCs (RIKEN Cell Bank, Japan) were cultured in Dulbecco's Modified Eagle Medium (DMEM) with high glucose content, 10% fetal bovine serum and 1% antibiotics (penicillin/streptomycin) at 37 ºC in a humidified atmosphere of 5 % CO_2. Cells were subcultured once a week before reaching confluence. In all experiments density of seeding was 10.000 cells/cm^2. Each experiment was performed in triplicate. The cell viability of the coatings was

evaluated in contact and non-contact mode, respectively by the assays LIVE/DEAD™ (Viability/Cytotoxicity kit, Invitrogen, Thermo Fisher Scientific) and MTT (3-(4,5-dimethylthiazol-2-yl)-2,5-diphenyl tetrazolium bromide) (Cell Proliferation Kit I, Roche). For the first analysis, the cells were seeded on the coatings' surface and also on the Ti-6Al-4V surface in DMEM medium, glass was used as control. The incubation was performed at 37°C in the presence of 5% CO_2 for 72 h. The cytotoxic control was treated with dimethyl sulfoxide (DMSO 20%) at 24 h. After the incubation time, a mixture of Calcein, AM (Invitrogen) and Ethidium homodimer-1 (Life technologies) (EthD-1) was added to each system, which were incubated for a further 4 h. Finally, the samples were observed using a fluorescence microscope (Nikon Eclipse 80i). MTT assay was performed to evaluate non-contact cytocompatibility of the different coatings, which were incubated under culture conditions for 72h, the medium was then removed and taken to culture p-96 multi-well plates with previously seeded cells, whereupon a new incubation at 37°C and with 5% CO_2 was carried out for 72 hours. After this time, MTT was added to all the samples, which were incubated for a further 4 h. Again, the cytotoxic control was treated with DMSO and, for the live control (100% viability), cells seeded on the well plate in clean culture medium (not exposed to the coatings), was used. Finally, the absorbance at 570 nm was measured in a spectrophotometer (Perkin Elmer Precisely, 1420 Multilabel Counter, VICTOR^3).

2.6. Statistical analysis

The results obtained for the Ag quantification, roughness and the residual stresses are shown as the mean ± standard deviation. Additionally, the results of the cell viability (MTT) and wettability test were analyzed using one-way analysis of variance, by means of a multiple comparison test (Tukey's) using the GraphPad Prims 6 XML software.

3. Results and discussion

3.1. Chemical composition, phases and crystallinity

TiN, HA-Ag and HA-Ag/TiN-Ti Coatings were deposited on Ti-6Al-4V by MS. Table 1 shows the Ti/N and Ca/P ratios, as well as the Ag atomic % in the coatings. The chemical composition of the TiN layer was effectively controlled, obtaining a Ti/N ratio very close to 1. In contrast, the Ca/P ratios for the HA-Ag and HA-Ag/TiN systems were slightly higher than the HA stoichiometric value (1.67). In addition, the alteration was less in the HA-Ag multi-layer coating deposited on the TiN layer than in the one deposited on the Ti-6Al-4V alloy. This indicates a surface effect of the atoms arrival from the target, behavior most likely associated with the greater reactivity and "Pauling electronegativity" of the titanium alloy than TiN, causing it to enter into preferential union with positive ions of Ca^{+2} and Ag^{+} rather than with the anions of $(PO_4)^{3-}$, resulting in a higher Ca/P ratio and higher Ag content [22]. On the other hand, the bias voltage of -20V applied to the substrate could have a repulsive effect on the negative ions, contributing to a higher Ca/P ratio in the multilayer coating, as well as to the preferential resputtering phenomenon of the phosphorus of the HA. This has been observed by other authors [23,24], who have reported changes in the chemical composition of HA coatings deposited by MS, obtaining Ca/P ratios from 1.5 to 3.8 as a function of the substrate polarization. In addition to the above, an increase in surface roughness was observed with the inclusion of the TiN-Ti interlayer, since it presented greater roughness than the substrate itself, as discussed below.

Table 1. Chemical composition analysis for the deposited coatings.

Coatings	Ti/N ratio	Ca/P ratio	Ag atomic % ± SD
TiN-Ti	0.96	---	---
HA-Ag	---	1.85	7.6 ± 0.01
HA-Ag/TiN-Ti	0.95	1.74	6.5 ± 0.01

Fig. 2 shows the micro-Raman spectra obtained for the TiN-Ti bilayer and the HA-Ag/TiN multi-layer coating. The following TiN characteristic vibration bands can be observed in Fig. 2a: I) dispersion in the acoustic range, with bands centered close to 230 cm^{-1} (transverse acoustic, TA) and 320 cm^{-1} (longitudinal acoustic, LO), generated by the vibration of Ti ions; II) dispersion in the optical range, a band centered at 590 cm^{-1} (longitudinal optical, LO), related to vibrations of nitrogen ions [25]**.** Fig. 2b shows the characteristic vibrations of the phosphate group $(PO_4)^{3-}$, with a non-degenerate main band present at 960 cm^{-1} (ν1). This vibration, as well as that observed close to 1060 cm^{-1} (ν3) which corresponds to the tension of the PO bond, are characteristics of HA, and can differentiate this compound from the other calcium phosphates, which present modifications or do not emit under these wavelengths [26,27]. Additionally, the spectrum shows the vibration in flexion of the O-P-O bond, which emits both around 470 cm^{-1} (ν2) and around 600 cm^{-1} (ν4), although these two vibrations were altered with the TiN band (LO). In the same way, the union of the (TA) and (longitudinal acoustic, LA) bands can be observed in this spectrum.

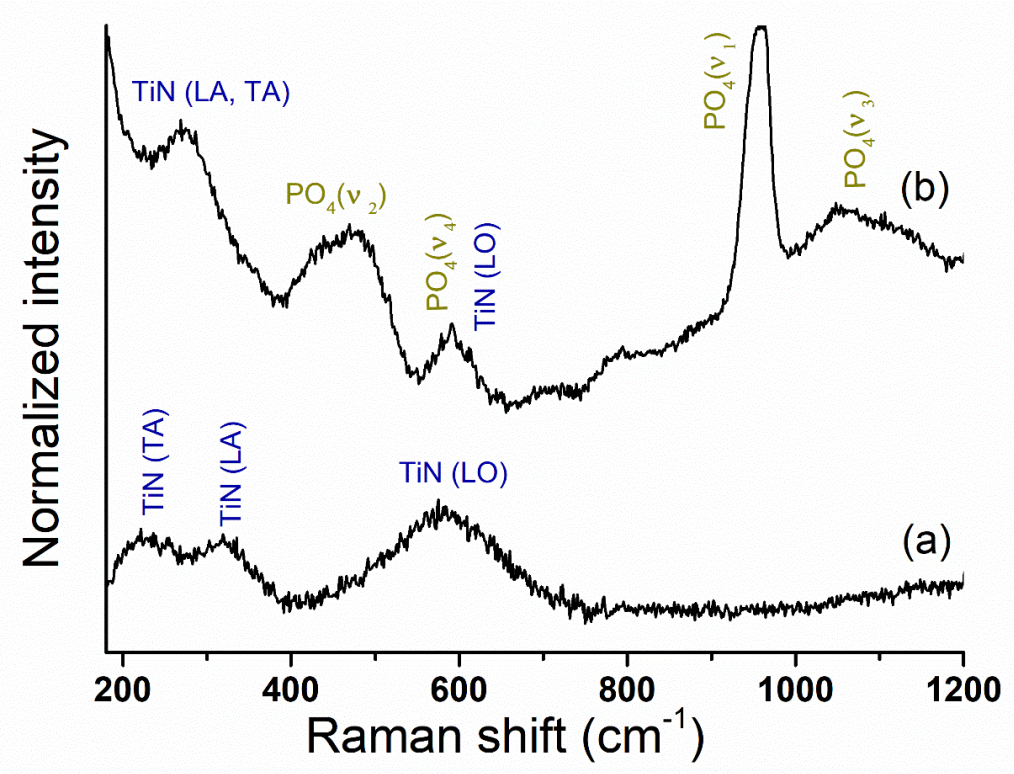

Figure 2. Raman spectra for: a) TiN-Ti coating and b) HA-Ag/TiN-Ti multi-layer coating.

Fig. 3 shows the diffractograms obtained for the HA-Ag and HA-Ag/TiN-Ti coatings between 16° and 34° 2Θ. In both diffractograms, two peaks are observed at 25.6° and 32.8°, which correspond to the crystallographic planes (002) and (112) of HA according to the ASTM card N°. 9-432. These slightly widened peaks could indicate the formation of nanocrystalline coatings [28]. Additionally, it is observed in both diffractograms that the preferential growth along the (112) plane was not altered with the surface change. In contrast, the peak related to the plane (002) did present modifications, registering a greater intensity in the diffractogram corresponding to the HA-Ag coating deposited on TiN than on the system obtained on the Ti-6Al-4V, indicating that there was greater crystallinity in the HA deposited on the TiN intermediate layer. This is very important, given that HA requires an adequate degree of crystallinity for implant applications, since increased crystallinity in the coating decreases its dissolution rate in biological medium [29], making

application of different post-deposit thermal treatments normally necessary in order to achieve the required degree of crystallinity [30]. However, during these processes, residual stresses can be generated in the HA coatings as a consequence of the difference between the coefficients of thermal expansion between them and the metallic substrate, which triggers the appearance of cracks and coating delamination [31].

Meanwhile, the formation of nanocrystalline coatings was proved by calculating the crystallite size with the Scherrer equation. For this, the FWHM of the peak corresponding to the preferential growth plane of the HA was used, as shown in Table 2. It is also observed that the ordered growth of the coatings is favored when they are deposited on the intermediate TiN layer rather than on the Ti-6Al-4V substrate, with a 7% increase in crystallite size recorded. In the literature, decreases in crystallite size have been reported as a function of substrate polarization, A.A. Ivanova *et al.* [28] obtained a change from nanocrystalline (crystallite size=26 nm) to amorphous in HA coatings after polarization of the substrates with -50V. In addition, M.A. Surmeneva *et al.* [32] reported a decrease in crystallite size from 30 nm to 15 nm for HA coatings deposited to 0V and -50V, respectively. This indicates that the behavior recorded in the present study could once again be related to changes in the Ti-6Al-4V surface charge generated by the TiN deposition, since this coating has lower reactivity and could act as a barrier layer, decreasing the effect of the holder polarization with bias voltage of -20 V during the deposition process, as discussed above. In addition, it is important to note that the crystallite size recorded for the two evaluated systems is higher than the values reported in the cited references and in some other similar works [3,33].

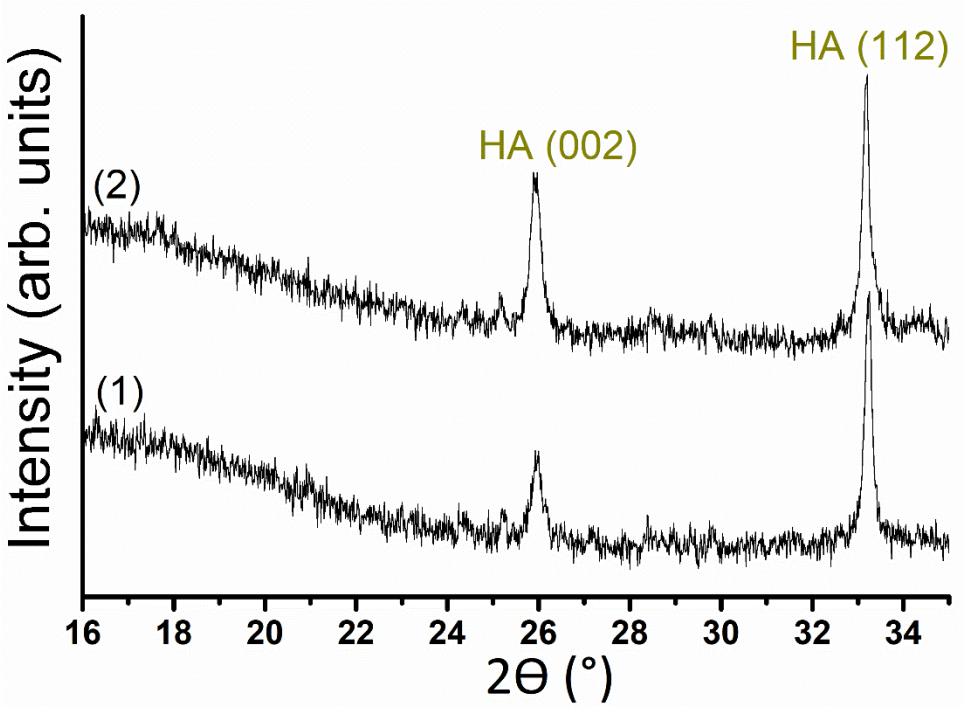

Figure 3. Diffractogram for: (1) HA-Ag and (2) HA-Ag/TiN-Ti coatings.

Table 2. FWHM and Crystallite size for the HA-Ag coatings deposited on Ti-6Al-4V and TiN-Ti.

HA-Ag coating deposited on:	FWHM (°)	Crystallite size (nm)
Ti-6Al-4V	0.21	42.4
TiN-Ti	0.19	45.3

3.2. Structure, morphology, roughness and wettability

Fig. 4 shows the SEM images of the surface and the cross-section view of the developed systems. The second of these was obtained by generating a ductile fracture in the coatings. In Fig. 4a the structure of the TiN-Ti coating is observed, with a columnar growth that starts from the Ti layer and is maintained along the TiN layer. At the surface level, it is possible to observe the cauliflower-type upper contour of the columns created on the surface of the TiN layer, a shape maintained for

all coatings observed. These results are similar to those obtained by the authors of reports [4,34] for TiN coatings deposited by MS. On the other hand, the multi-layer HA-Ag coating deposited directly on Ti-6Al-4V exhibits a dense and homogeneous structure, which loses its columnar appearance and has a high level of fragility (Fig. 4b), with evidence of many cracks and detachment of the substrate. The presence of the multiple HA and Ag deposited layers was not revealed in this coating, probably because of the nanometric thickness of the Ag layers and the low resolution achieved with the SEM equipment used. Finally, the surface and cross section image of the multi-layer coating composed of HA-Ag/TiN-Ti is presented in Fig. 4c. Here, it is observed that the TiN-Ti intermediate layer is perfectly joined both to the HA-Ag coating and to the metallic substrate, suggesting a greater adherence and mechanical stability of the entire coating system. In general terms, in Figs. 4, from a) to c) an increase in the roughness, grain size and density of the coating is observed as well as a significant increase in the coating adhesion to the substrate with the inclusion of the TiN-Ti interlayer.

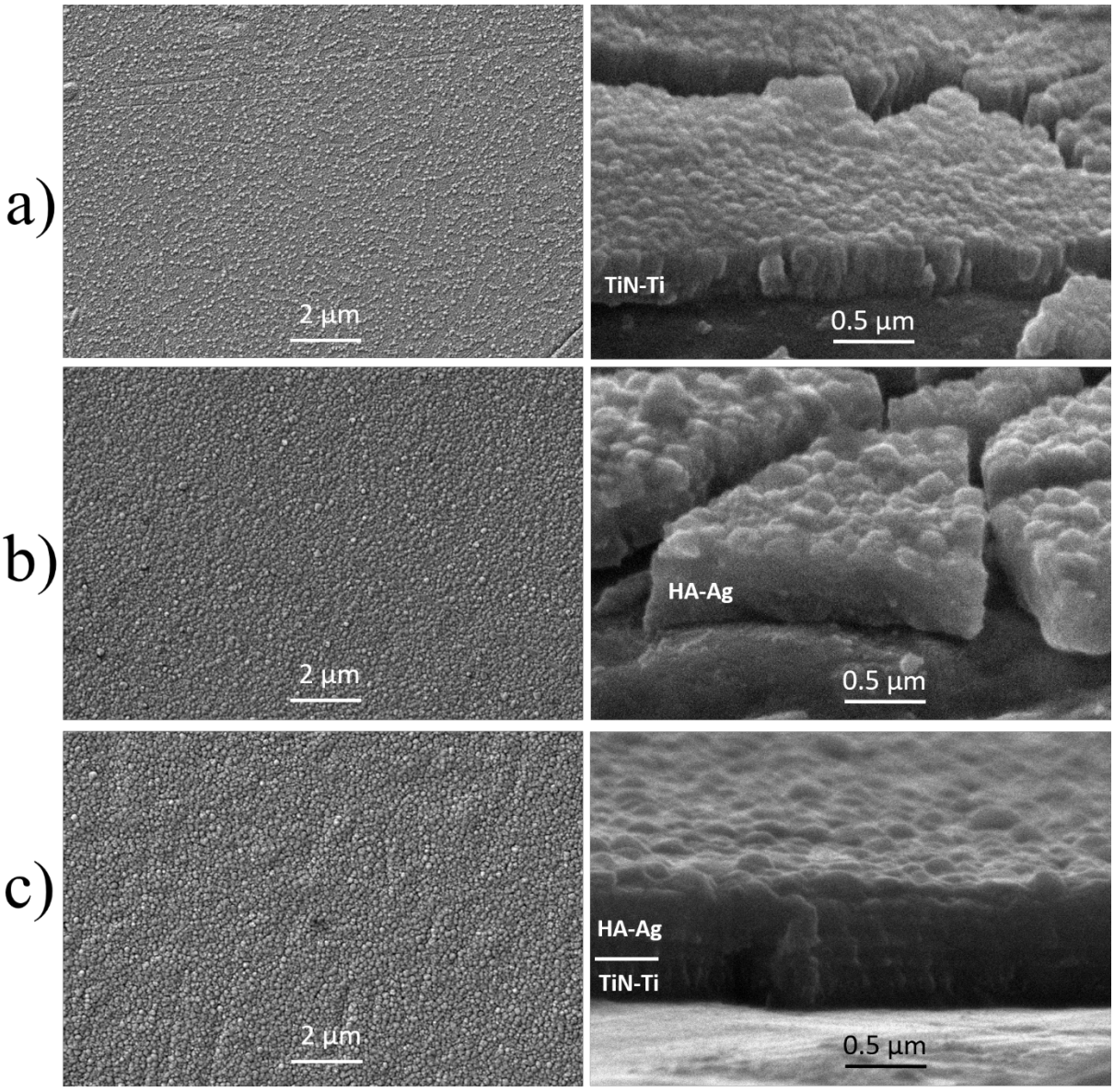

Figure 4. Surface morphology (x8.000) and cross-section view (x40.000) obtained from a secondary electrons beam for: a) TiN-Ti coating, b) HA-Ag coating and c) HA-Ag/TiN-Ti coating.

Fig. 5 shows the results of the FIB-FESEM analysis for the HA-Ag and HA-Ag/TiN-Ti coatings. Here, the trench generated with ion beam allowed us to observe in detail both the presence of the HA and Ag layers as well as the intermediate TiN-Ti layers. In Figs. 5a and b it is possible to see

the 4 Ag layers, which each have approximately 35 nm thickness and are continuous along the generated cut, deposited between 5 HA layers with approximately 90 nm thickness. The low uniformity of the Ag layers in some areas could be related to the diffusion process of Ag towards the adjacent HA layers, generated as a product of the deposition process at 200°C. Meanwhile, the TiN and Ti layers, with a high uniformity degree and approximately 230 nm and 80 nm thickness respectively, are observed in Fig. 5b. These FESEM images confirm the design of the coating system suggested in Fig. 1.

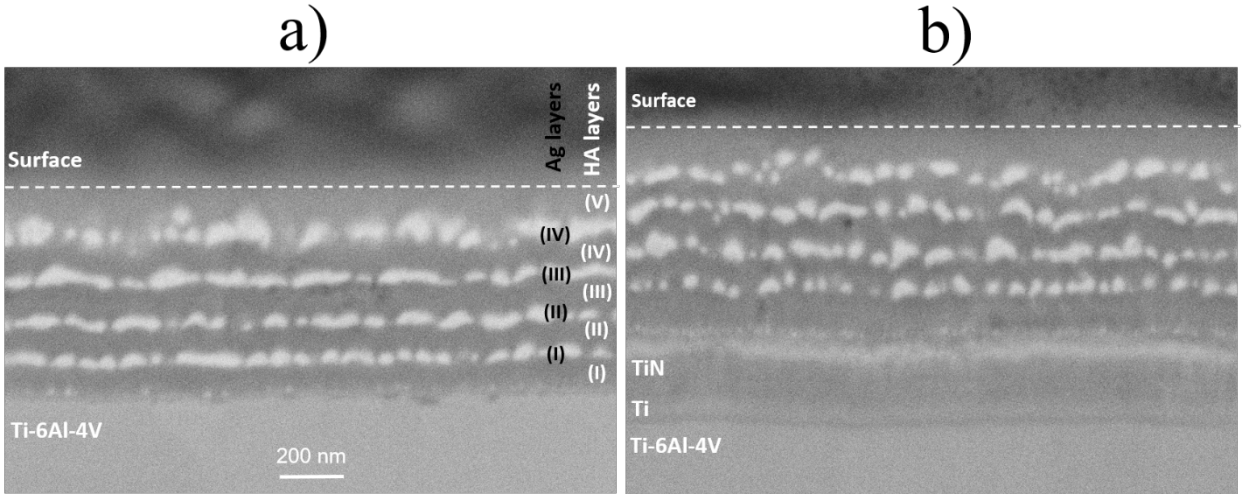

Figure 5. The FIB-FESEM cross-sectional image obtained from back-scattered electrons for: a) HA-Ag/Ti-6Al-4V and b) HA-Ag/TiN-Ti/Ti-6Al-4V. x60.000.

In addition to the chemical composition, crystallinity and morphology, surface characteristics such as roughness and wettability are very important in coatings with potential use in implants since they can play a critical role in the cell adhesion process [35,36]. Fig. 6 shows the values obtained for roughness in Mean Square Root (RMS) of Ti-6Al-4V and the deposited coatings. The lowest value was recorded for the substrate used (mirror finish), where roughness increased after the deposition of both the TiN-Ti and HA-Ag coatings onto it with a slightly higher value recorded

for the latter system. The highest roughness was obtained for the HA-Ag/TiN-Ti multi-layer coating, in which the HA-Ag layer grew on a rougher surface (TiN, with an RMS of approximately 8.4 nm) in comparison with the HA-Ag coating which was deposited on Ti-6Al-4V (RMS of approximately 3.6 nm). According to D.D. Deligianni *et al*. [37], the increase in the roughness of Ti-6Al-4V can favor cell adhesion, proliferation and differentiation.

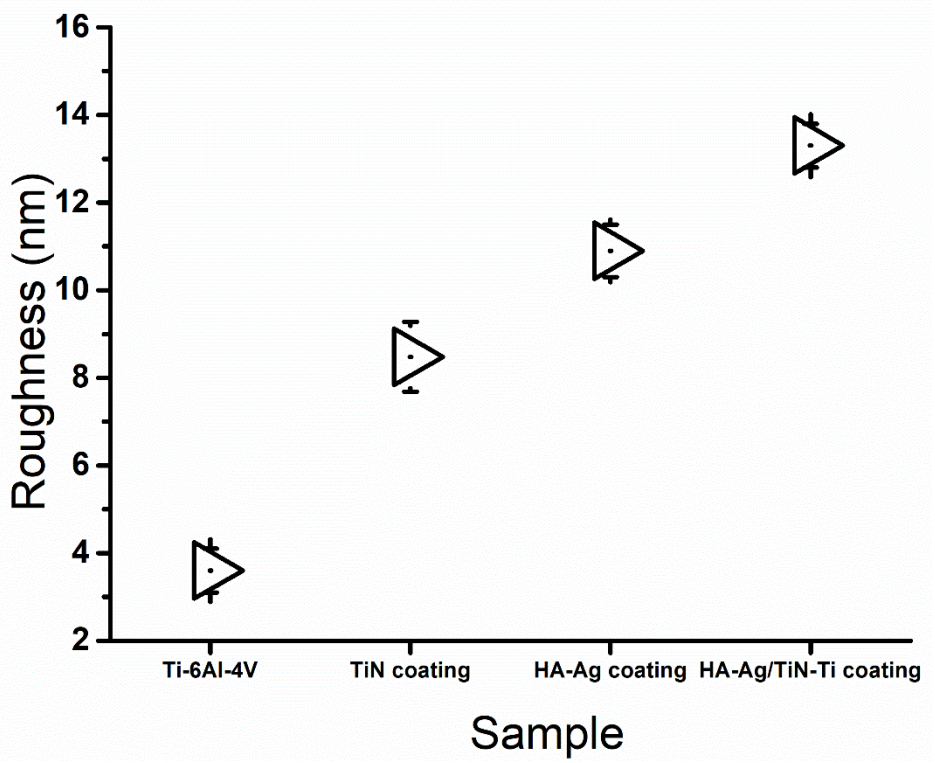

Figure 6. RMS values for the used substrate and the deposited systems.

Fig. 7 shows the water contact angle and the surface free energy of the Ti-6Al-4V and the deposited coatings. Here, it can be observed that both the TiN coating and the substrate used have hydrophobic behavior, according to the authors of the report [38], since the contact angle was greater than 90°. On the other hand, the HA-Ag coatings showed a greater water affinity, obtaining

a significant reduction in the contact angle and presenting a hydrophilic character. Additionally, the surface free energy was greater for these last two systems than for the TiN coating and the substrate. The decrease in the contact angle could be related to the presence of both electronegative anions of $(PO_4)^{3-}$ and OH^- in HA, which tend to attract strongly H^+ ions of water molecules [11]. C.G García *et al.* [39] decreased the water contact angle from 89° to 45° in ethylacrylamide membranes by a hydroxylation process.

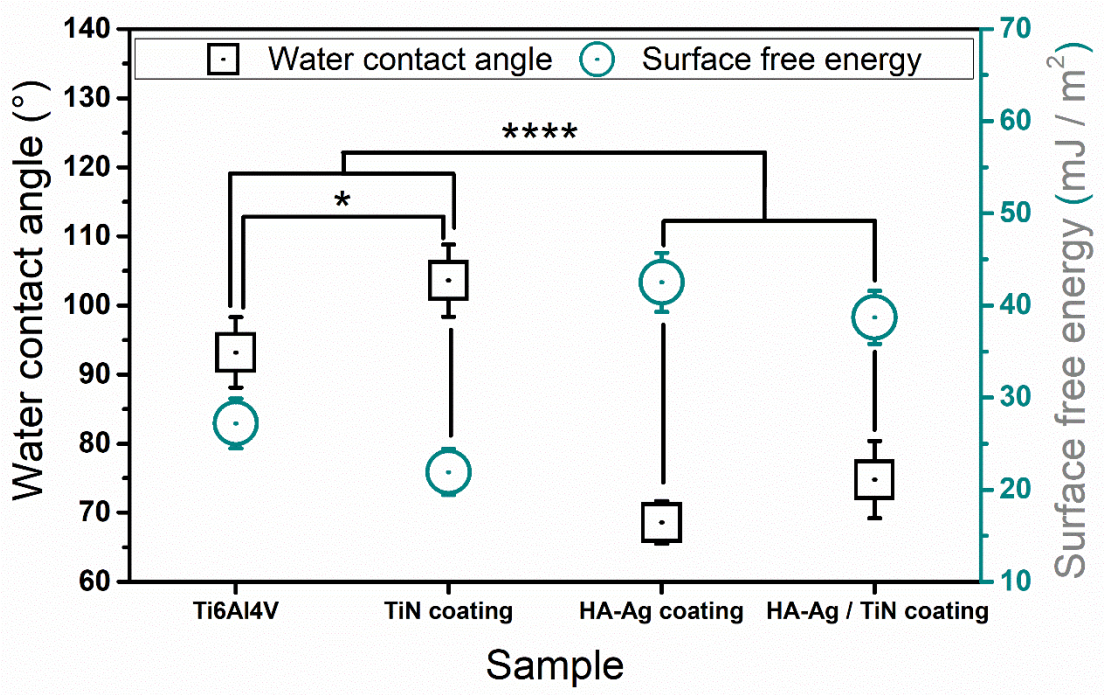

Figure 7. Water contact angle and surface free energy for the used substrate and the deposited systems.

3.3. Residual stresses and adhesion

The residual stresses of the HA-Ag and HA-Ag/TiN-Ti coatings are shown in Fig. 8. There is an approximate reduction of 36% in the compressive stresses of the HA-Ag coating after the

intermediate TiN-Ti bilayer incorporation. This result indicates that there was a good affinity both between the HA-Ag layer and the TiN-Ti coating, and between the latter and the Ti-6Al-4V substrate. This relief of tensions could be related to the decrease between the difference of the thermal expansion coefficients of HA and Ti-6Al-4V (11.5×10^{-6} K^{-1} and 8.50×10^{-6} K^{-1}, respectively) with the incorporation of TiN which has an intermediate value of 9.35×10^{-6} K^{-1} [9,40], causing greater energy dissipation and relief of tensions during the formation of the composite coating. This is important since the compressive tension produces a normal tensile stress to the plane of the coating, which acts on any pre-existing flaws and defects to promote the delamination of the coating [41].

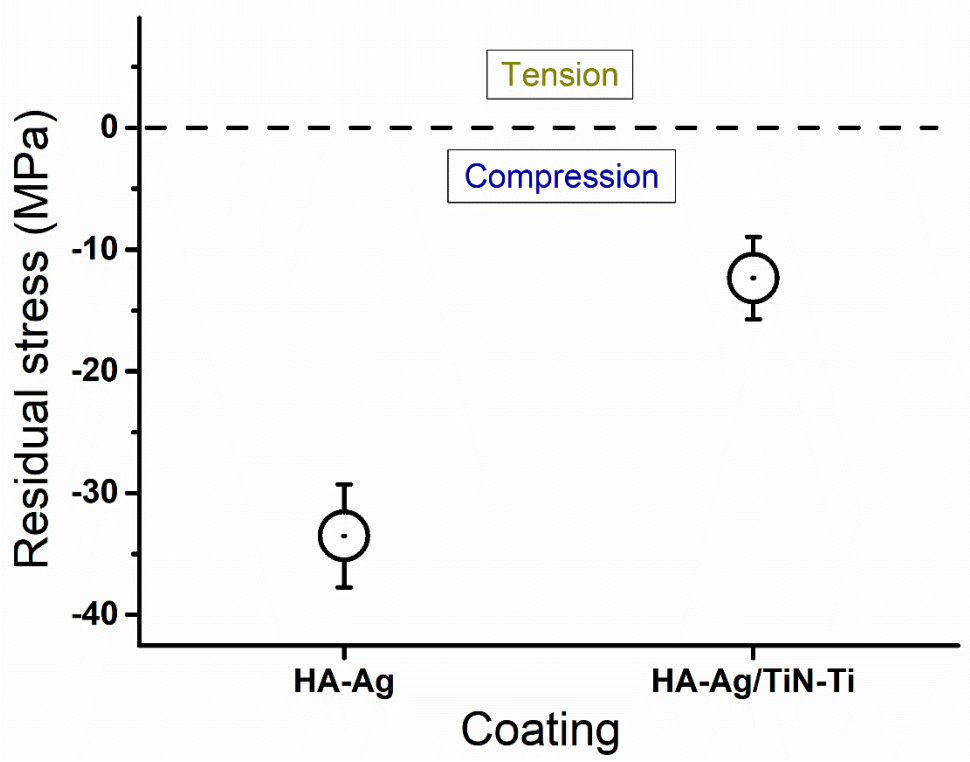

Figure 8. Residual stresses of HA-Ag and HA-Ag/TiN-Ti coatings.

The friction records and applied load as a function of the scratch distance for HA-Ag and HA-Ag/TiN-Ti coatings are presented in Fig. 9. For this first system, a critical load (L_C) of 114 mN was determined, which caused the adhesive failure of the coating, Fig. 9a. This result is interpreted as an abrupt change in the friction coefficient recorded at a distance of around 650 μm, which is generated by the change of surface in contact with the diamond tip during this mechanical evaluation, in this case a coating-substrate transition. In contrast, the adhesive failure between the HA-Ag/TiN-Ti coating and the Ti-6Al-4V substrate generated an L_C of 150 mN, Fig. 9b. This result indicates that there was a 32% increase in the adhesion of the HA-Ag coating to the metal substrate with the TiN incorporation, which is related to the decrease in residual stress recorded for this multi-layer system. These stresses can reduce the cohesion and adhesion of the coatings, which is evidenced by exerting a mechanical load on them [42]. Y.C. Yang *et al.* [43] reported decreases in the bonding strength in HA coatings deposited on Ti-6Al-4V by plasma-sprayed as a function of the increase in compressive residuals stress, which were generated by means the increase in the deposition temperature due to the differences in the thermal expansion coefficients between the coating and the substrate.

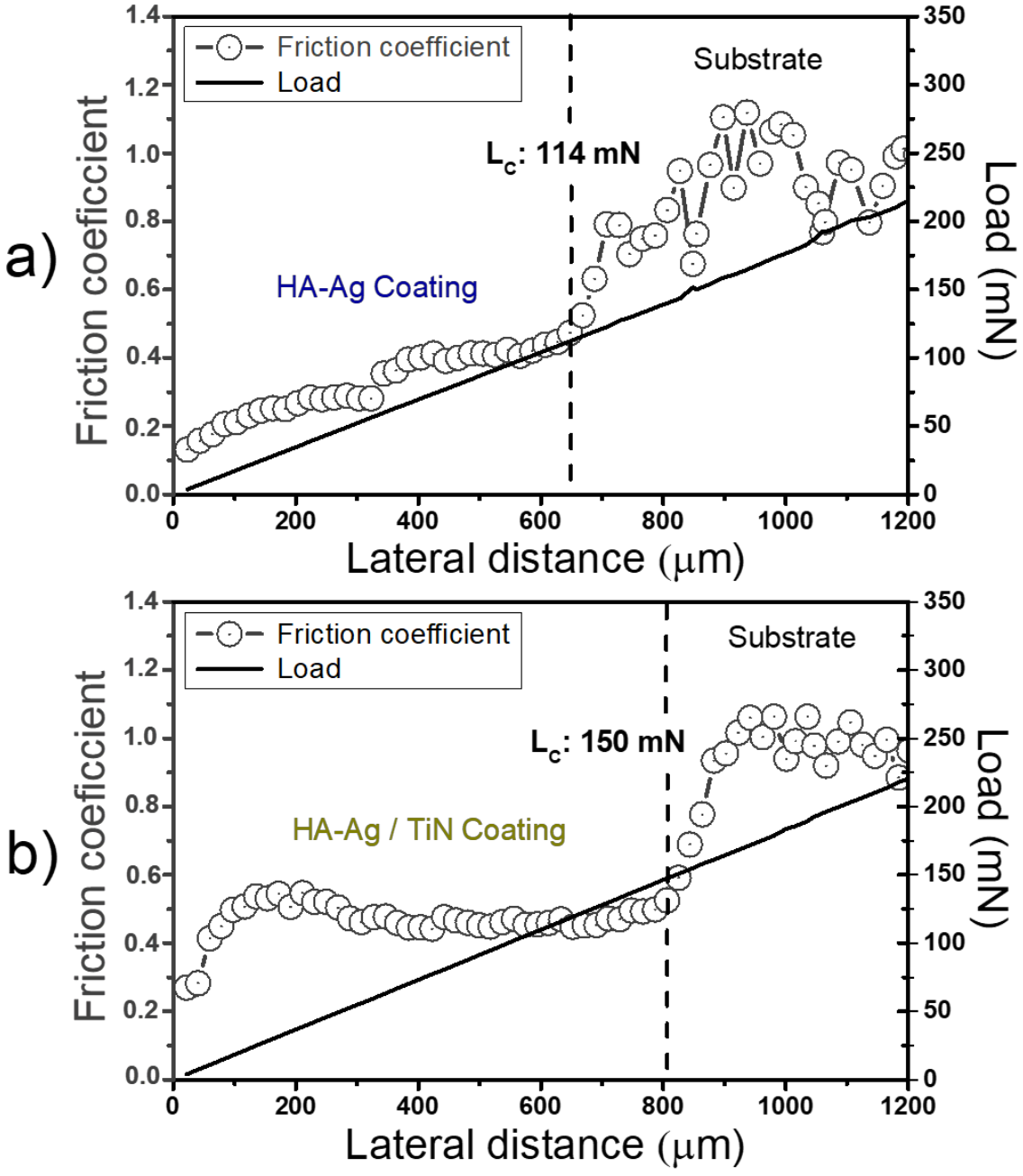

Figure 9. Micro-scratch test result: friction and load vs lateral distance of: a) HA-Ag and b) HA-Ag/TiN-Ti coatings.

3.4. Cytotoxicity analysis

Fig. 10 shows the results of the cell viability test carried out by the LIVE/DEAD™ assay. Figs. 10a and b show the respective images of cytotoxic control (cell death, loss of plasma membrane integrity) and cell control (high intracellular esterase activity). In addition, Fig. 10c shows the image of the cells on the Ti-6Al-4V surface. In contrast, images of the cells seeded on the HA-Ag and HA-Ag/TiN-Ti coatings are appreciated in Figs. 10d and e. In the images corresponding to the substrate and the coatings a green fluorescent staining can be seen in the cells, indicating that their intracellular esterase activity was not affected by contact with the coatings' surface. On the other hand, significant differences in the cell viability of these coatings were not found by the MTT assay where values close to 80% for all systems were recorded (Fig. 11) and where the metabolic activity of mMSCs exposed to the medium containing dissolved elements of the coatings was evaluated. The results obtained indicate that HA-Ag and HA-Ag/TiN-Ti coatings are potentially non-toxic to mMSCs, since the amount of Ag released to the medium through the structure or dissolution of the HA layers was not enough to reach cytotoxic concentrations. In a previous study, we found an Ag cumulative concentration $< 2\times10^{-3}$ mg/L at 72 h of immersion in PBS medium [44], which is much lower than that reported by the authors of the study [15], who obtained cytotoxic effects at Ag concentrations > 2.5 mg/L.

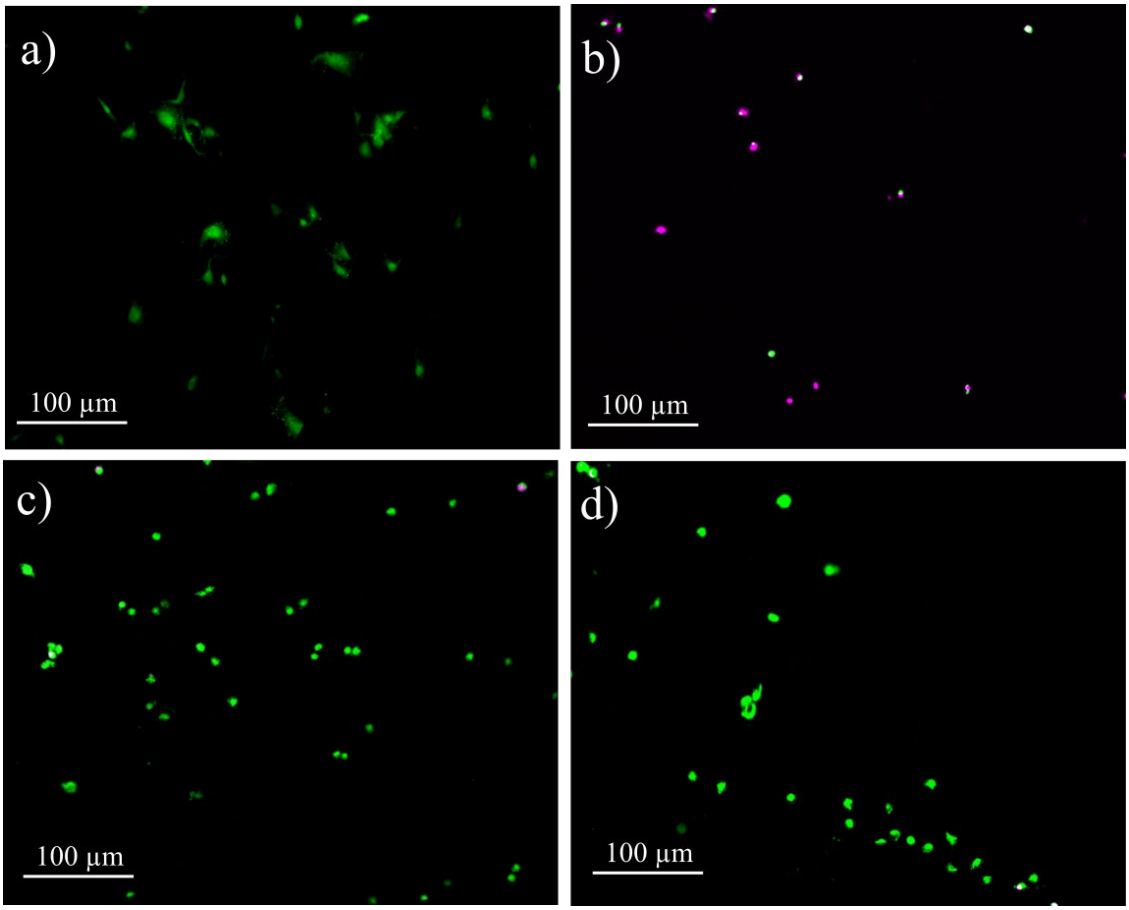

Figure10. Fluorescence images showing live cells stained with calcein-AM (green) and dead cells with EthD-1 (red); a) live control (100% viability), b) cytotoxicity control, c) HA-Ag coating and d) HA-Ag/TiN-Ti multi-layer coating.

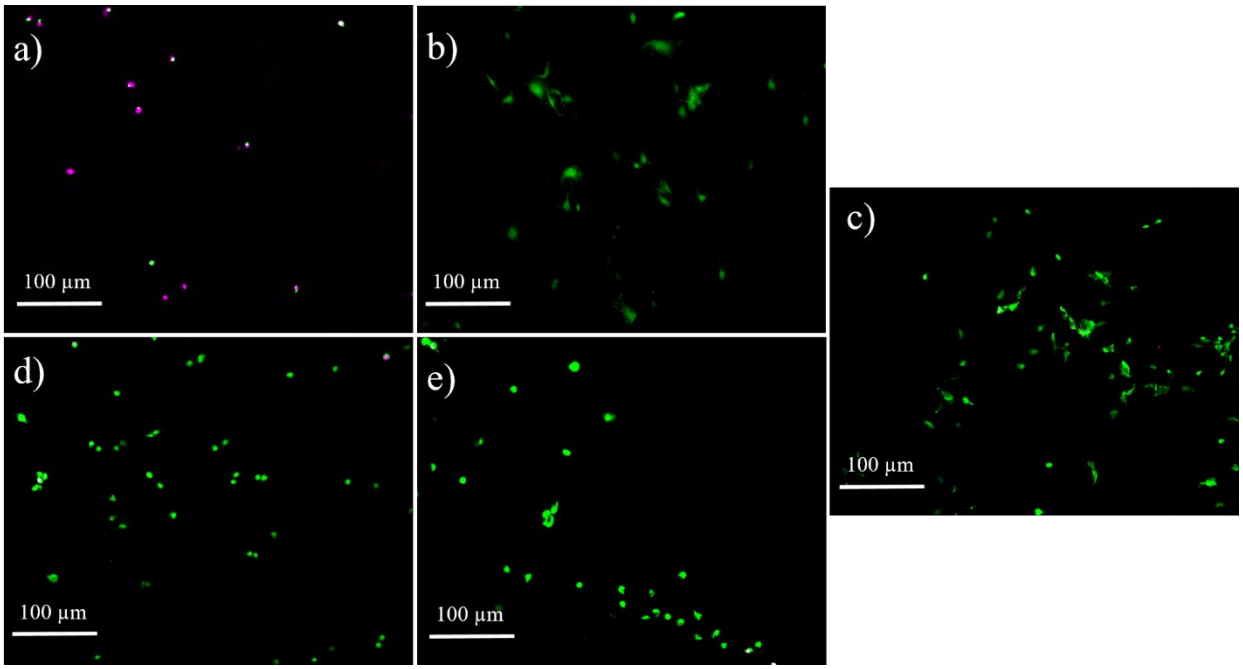

Figure 10. Fluorescence images showing live cells stained with calcein-AM (green) and dead cells with EthD-1 (red); a) live control (100% viability), b) cytotoxicity control, c) Ti-6Al-4V substrate, d) HA-Ag coating and e) HA-Ag/TiN-Ti multi-layer coating

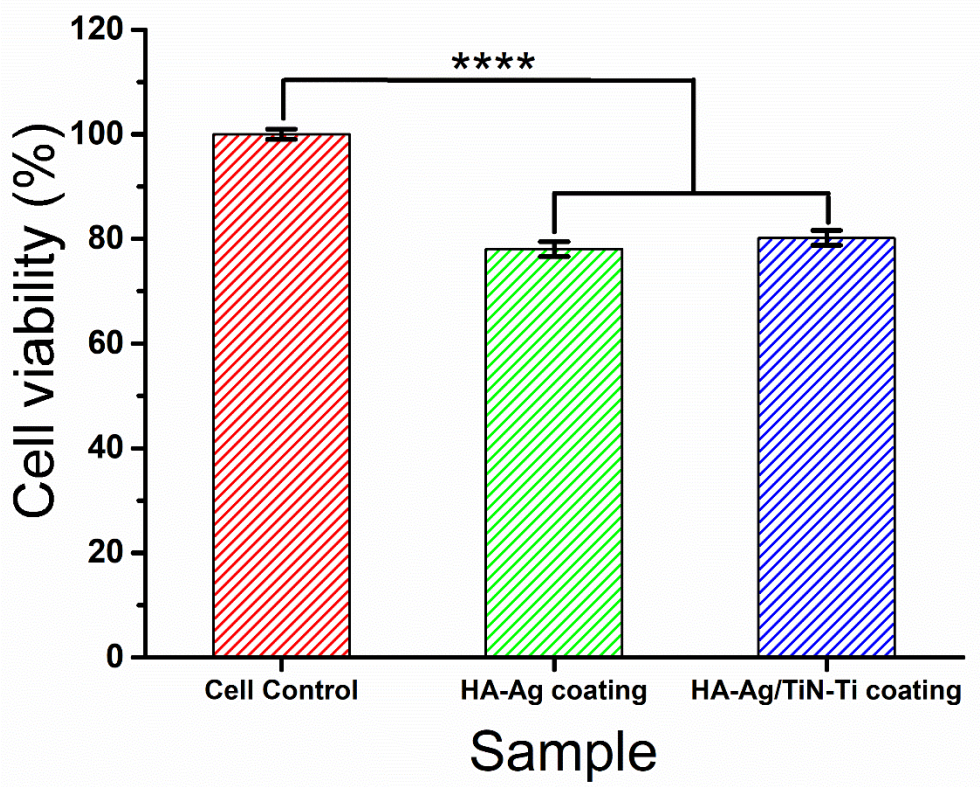

Figure 11. Cell viability of the HA-Ag and HA-Ag/TiN-Ti coatings by MTT assay. Statistics are shown as mean ± standard deviation, n=3, ****P < 0.0001.

4. Conclusions

The incorporation of an intermediate TiN-Ti bilayer was found to affect the chemical composition, crystallinity, roughness and mechanical properties of a multilayer HA-Ag coating deposited on Ti-6Al-4V. EDS analysis showed a decrease in the Ca/P ratio when the HA-Ag coating was deposited on the intermediate TiN layer. This is possibly related to a decrease in the surface charge (Pauling electronegativity) of the substrate, and a lower effect of the bias voltage when the substrate was coated with a TiN layer, which generates the attraction of positive ions of Ca^{+2} or the preferential repulsion of certain elements such as negative $(PO_4)^{3-}$ ions towards the substrate surface. Additionally, there was an increase in the crystallinity of the HA after TiN incorporation, which

can decrease the HA dissolution rate, favoring its osteogenesis and cell growth processes in biological medium. The roughness of the Ti-6Al-4V increased with the deposition of the different coatings developed, also achieving a change from hydrophobic to hydrophilic with the deposition of HA-Ag and HA-Ag/TiN-Ti coatings. Additionally, the incorporation of the TiN-Ti intermediate bilayer increased the HA crystallite size by 7%, decreased the residual stresses of the HA-Ag on the substrate by 36% and improved adhesion by 32%. Furthermore, it was possible to determine the potentially non-toxic character of the coatings through biological evaluation, obtaining a cell viability close to 80% for the two developed systems. The results obtained are very favorable in terms of the potential use of these systems in the biomedical field, since by depositing the biocompatible and antibacterial coating of HA-Ag/TiN-Ti, superficial modification and functionalization of the Ti-6Al-4V alloy, widely used for the manufacture of surgical prostheses, was achieved.

Acknowledgments

We thank the University of Antioquia, the Centro de Investigación, Innovación y Desarrollo de materiales (CIDEMAT) group, the Departamento Administrativo de Ciencia, Tecnología e Innovación (COLCIENCIAS) for financing the Project 15-1696, the scholarship program of Enlazamundos, PR and JLGR acknowledge financial support from the Spanish Ministry of Economy and Competitiveness (MINECO) through the project MAT2016-76039-C4-1-R (AEI/FEDER, UE) (including the FEDER financial support). CIBER-BBN is an initiative funded by the VI National R&D&I Plan 2008–2011, Iniciativa Ingenio 2010, Consolider Program. CIBER Actions are financed by the Instituto de Salud Carlos III with assistance from the European Regional Development Fund.

References

[1] H. Melero, J. Fernández, J.M. Guilemany, Recubrimientos bioactivos: Hidroxiapatita y titania, Biomecánica. 19 (2011) 35–48. http://hdl.handle.net/2099/12325.

[2] K. Ozeki, T. Yuhta, Y. Fukui, H. Aoki, Phase composition of sputtered films from a hydroxyapatite target, Surf. Coat. Technol. 160 (2002) 54–61.

[3] V. Nelea, C. Morosanu, M. Iliescu, I.N. Mihailescu, Microstructure and mechanical properties of hydroxyapatite thin films grown by RF magnetron sputtering, Surf. Coatings Technol. 173 (2003) 315–322. doi:10.1016/S0257-8972(03)00729-1.

[4] E. Mohseni, E. Zalnezhad, A.R. Bushroa, A.M. Hamouda, B.T. Goh, G.H. Yoon, Ti/TiN/HA Coating on Ti-6Al-4V for Biomedical Applications, Ceram. Int. 41 (2015) 14447–14457. doi:10.1016/j.ceramint.2015.07.081.

[5] V. Nelea, C. Morosanu, M. Bercu, I.N. Mihailescu, Interfacial titanium oxide between hydroxyapatite and TiAlFe substrate, J. Mater. Sci. Mater. Med. 18 (2007) 2347–2354. doi:10.1007/s10856-007-3135-1.

[6] M.S. Tkachev, E.S. Melnikov, M.A. Surmeneva, A.A. Sharonova, R.A. Surmenev, O.S. Korneva, I.A. Shulepov, K. Loza, M. Epple, Adhesion properties of a three-layer system based on RF-magnetron sputter deposited calcium-phosphate coating and silver nanoparticles, Proc. - 2016 11th Int. Forum Strateg. Technol. IFOST 2016. (2017) 88–90. doi:10.1109/IFOST.2016.7884197.

[7] E. Mohseni, E. Zalnezhad, a. R. Bushroa, Comparative investigation on the adhesion of hydroxyapatite coating on Ti-6Al-4V implant: A review paper, Int. J. Adhes. Adhes. 48 (2014) 238–257. doi:10.1016/j.ijadhadh.2013.09.030.

[8] A. Sargeant, T. Goswami, Hip implants – Paper VI – Ion concentrations, Mater. Des. 28 (2007) 155–171. doi:https://doi.org/10.1016/j.matdes.2005.05.018.

[9] J. Qi, Y. Yang, M. Zhou, Z. Chen, K. Chen, Effect of transition layer on the performance of hydroxyapatite / titanium nitride coating developed on Ti-6Al-4V alloy by magnetron sputtering, Ceram. Int. 45 (2019) 4863–4869. doi:10.1016/j.ceramint.2018.11.183.

[10] S. Ghasemi, A. Shanaghi, P.K. Chu, Nano mechanical and wear properties of multi-layer Ti/TiN coatings deposited on Al 7075 by high-vacuum magnetron sputtering, Thin Solid Films. 638 (2017) 96–104. doi:10.1016/j.tsf.2017.07.049.

[11] E.S. Thian, J. Huang, Z.H. Barber, S.M. Best, W. Bonfield, Surface modification of magnetron-sputtered hydroxyapatite thin films via silicon substitution for orthopaedic and dental applications, Surf. Coatings Technol. 205 (2011) 3472–3477. doi:10.1016/j.surfcoat.2010.12.012.

[12] A. Vladescu, I. Birlik, V. Braic, M. Toparli, E. Celik, F. Ak Azem, Enhancement of the mechanical properties of hydroxyapatite by SiC addition, J. Mech. Behav. Biomed. Mater. 40 (2014) 362–368. doi:10.1016/j.jmbbm.2014.08.025.

[13] F.A. Azem, A. Kiss, I. Birlik, V. Braic, C. Luculescu, A. Vladescu, The corrosion and bioactivity behavior of SiC doped hydroxyapatite for dental applications, Ceram. Int. 40 (2014) 15881–15887. doi:10.1016/j.ceramint.2014.07.116.

[14] C.S. Ciobanu, S.L. Iconaru, P. Le Coustumer, L.V. Constantin, D. Predoi, Antibacterial activity of silver-doped hydroxyapatite nanoparticles against gram-positive and gram-negative bacteria, Nanoscale Res. Lett. 7 (2012) 1–9.

[15] A. Peetsch, C. Greulich, D. Braun, C. Stroetges, H. Rehage, B. Siebers, M. Köller, M. Epple, Silver-doped calcium phosphate nanoparticles: Synthesis, characterization, and toxic effects toward mammalian and prokaryotic cells, Colloids Surfaces B Biointerfaces. 102 (2013) 724–729. doi:10.1016/j.colsurfb.2012.09.040.

[16] A. Quirama, A.M. Echavarría, J.M. Meza, J. Osorio, G. Bejarano G, Improvement of the mechanical behavior of the calcium phosphate coatings deposited onto Ti6Al4V alloy using an intermediate TiN/TiO2 bilayer, Vacuum. 146 (2017) 22–30. doi:https://doi.org/10.1016/j.vacuum.2017.09.024.

[17] E. Contreras, Y. Galindez, M.A. Rodas, G. Bejarano, M.A. Gómez, CrVN/TiN nanoscale multilayer coatings deposited by DC unbalanced magnetron sputtering, Surf. Coatings Technol. 332 (2017) 214–222. doi:10.1016/j.surfcoat.2017.07.086.

[18] J.A. Lenis, F.M. Hurtado, M.A. Gómez, F.J. Bolívar, Effect of thermal treatment on structure , phase and mechanical properties of hydroxyapatite thin fi lms grown by RF magnetron sputtering, Thin Solid Films. 669 (2019) 571–578. doi:10.1016/j.tsf.2018.11.045.

[19] A.M. Sofronia, R. Baies, E.M. Anghel, C.A. Marinescu, S. Tanasescu, Thermal and structural characterization of synthetic and natural nanocrystalline hydroxyapatite, Mater. Sci. Eng. C. 43 (2014) 153–163. doi:10.1016/j.msec.2014.07.023.

[20] M. Żenkiewicz, Methods for the Calculation of Surface Free Energy of Solids, J. Achiev. Mater. Manuf. Eng. 24 (2007) 137.

[21] S. Shiri, P. Ashtijoo, A. Odeshi, Q. Yang, Evaluation of Stoney equation for determining the internal stress of DLC thin films using an optical profiler, Surf. Coatings Technol. 308 (2016) 98–100. doi:10.1016/J.SURFCOAT.2016.07.098.

[22] J. Barry, A. Cowley, P. Mcnally, D. Dowling, Influence of substrate metal alloy type on the properties of hydroxyapatite coatings deposited using a novel ambient temperature deposition technique, J. Biomed. Mater. Res. A. 102 (2014) 871–879. doi:10.1002/jbm.a.34755.

[23] R.A. Surmenev, M.A. Surmeneva, K.E. Evdokimov, V.F. Pichugin, T. Peitsch, M. Epple, The influence of the deposition parameters on the properties of an rf-magnetron-deposited nanostructured calcium phosphate coating and a possible growth mechanism, Surf. Coatings Technol. 205 (2011) 3600–3606. doi:10.1016/j.surfcoat.2010.12.039.

[24] M.A. Surmeneva, A.A. Sharonova, S. Chernousova, O. Prymak, K. Loza, M.S. Tkachev, I.A. Shulepov, M. Epple, R.A. Surmenev, Incorporation of silver nanoparticles into magnetron-sputtered calcium phosphate layers on titanium as an antibacterial coating, Colloids Surfaces B Biointerfaces. 156 (2017) 104–113. doi:10.1016/j.colsurfb.2017.05.016.

[25] C.P. Constable, J. Yarwood, W. Mu, Raman microscopic studies of PVD hard coatings, Surf. Coat. Technol. 119 (1999) 155–159. doi:10.1016/S0257-8972(99)00072-9.

[26] R. Cuscó, F. Guitián, S. de Aza, L. Artús, S. de Aza, L. Artús, Differentiation between hydroxyapatite and β-tricalcium phosphate by means of μ-Raman spectroscopy, J. Eur. Ceram. Soc. 18 (1998) 1301–1305. doi:http://dx.doi.org/10.1016/S0955-2219(98)00057-0.

[27] G.S. Mandair, M.D. Morris, Contributions of Raman spectroscopy to the understanding of bone strength, Bonekey Rep. 4 (2015) 1–8. doi:10.1038/bonekey.2014.115.

[28] A.A. Ivanova, M.A. Surmeneva, I.Y. Grubova, A.A. Sharonova, V.F. Pichugin, M. V. Chaikina, V. Buck, O. Prymak, M. Epple, R.A. Surmenev, Influence of the substrate bias on the stoichiometry and structure of RF-magnetron sputter-deposited silver-containing calcium phosphate coatings, Materwiss. Werksttech. 44 (2013) 218–225. doi:10.1002/mawe.201300101.

[29] K. Ozeki, T. Yuhta, H. Aoki, I. Nishimura, Y. Fukui, Crystal chemistry of hydroxyapatite

deposited on titanium by sputtering technique, Biomed. Mater. Eng. 10 (2000) 221–227. http://www.scopus.com/inward/record.url?eid=2-s2.0-0033635868&partnerID=40&md5=42941a64a2b4ad2e0216f526a350a0dd.

[30] Y. Yonggang, J.G.C. Wolke, L. Yubao, J.A. Jansen, The influence of discharge power and heat treatment on calcium phosphate coatings prepared by RF magnetron sputtering deposition, J. Mater. Sci. Mater. Med. 18 (2007) 1061–1069. doi:10.1007/s10856-007-0119-0.

[31] R. Xin, Y. Leng, J. Chen, Q. Zhang, A comparative study of calcium phosphate formation on bioceramics in vitro and in vivo, Biomaterials. 26 (2005) 6477–6486. doi:10.1016/j.biomaterials.2005.04.028.

[32] M.A. Surmeneva, A.I. Tyurin, T.M. Mukhametkaliyev, T.S. Pirozhkova, I.A. Shuvarin, M.S. Syrtanov, R.A. Surmenev, Enhancement of the mechanical properties of AZ31 magnesium alloy via nanostructured hydroxyapatite thin films fabricated via radio-frequency magnetron sputtering, J. Mech. Behav. Biomed. Mater. 46 (2015) 127–136. doi:10.1016/j.jmbbm.2015.02.025.

[33] M.A. Surmeneva, M. V. Chaikina, V.I. Zaikovskiy, V.F. Pichugin, V. Buck, O. Prymak, M. Epple, R. a. Surmenev, The structure of an rf-magnetron sputter-deposited silicate-containinghydroxyapatite-based coating investigated by high-resolution techniques, Surf. Coatings Technol. 218 (2013) 39–46. doi:10.1016/j.surfcoat.2012.12.023.

[34] M. Polok, M. Adamiak, Structure and properties of wear resistance PVD coatings deposited onto X37CrMoV5-1 type hot work steel, Mater. Process. Technol. 165 (2005) 843–849. doi:10.1016/j.jmatprotec.2005.02.164.

[35] A.R.A. Sagari, Ca-P-O thin film preparation, modification and characterisation, Ph.D thesis, University of Jyväskylä, 2011. https://jyx.jyu.fi/bitstream/handle/123456789/37195/Arcot_Rajashekar-Ananda-2011.pdf?sequence=1.

[36] S.R. Paital, N.B. Dahotre, Calcium phosphate coatings for bio-implant applications: Materials, performance factors, and methodologies, Mater. Sci. Eng. R Reports. 66 (2009) 1–70. doi:10.1016/j.mser.2009.05.001.

[37] D.D. Deligianni, N. Katsala, S. Ladas, D. Sotiropoulou, J. Amedee, Y.F. Missirlis, Effect of surface roughness of the titanium alloy Ti-6Al-4V on human bone marrow cell response

and on protein adsorption, Biomaterials. 22 (2001) 1241–1251.

[38] A.M. Echavarría, P. Rico, J.L. Gómez Ribelles, M.A. Pacha-Olivenza, M.C. Fernández-Calderón, G. Bejarano-G, Development of a Ta/TaN/TaNx(Ag)y/TaN nanocomposite coating system and bio-response study for biomedical applications, Vacuum. 145 (2017) 55–67. doi:10.1016/j.vacuum.2017.08.020.

[39] C.G. García, L.L. Ferrus, D. Moratal, M.M. Pradas, M.S. Sánchez, Poly(L-lactide) substrates with tailored surface chemistry by plasma copolymerisation of acrylic monomers, Plasma Process. Polym. 6 (2009) 190–198. doi:10.1002/ppap.200800112.

[40] W.. Perdok, J. Christoffersen, J. Arends, The thermal lattice expansion of calcium hydroxyapatite, J. Cryst. Growth. 80 (1987) 149–154.

[41] A.G. Evans, G.B. Crumley, R.E. Demaray, On the mechanical behavior of brittle coatings and layers, Oxid. Met. 20 (1983) 193–216. doi:https://doi.org/10.1007/BF00656841.

[42] ASTM C1624-05, Standard Test Method for Adhesion Strength and Mechanical Failure Modes of, Astm. 05 (2015) 1–29. doi:10.1520/C1624-05R15.Scope.

[43] Y.C. Yang, E. Chang, Influence of residual stress on bonding strength and fracture of plasma-sprayed hydroxyapatite coatings on Ti-6Al-4V substrate, Biomaterials. 22 (2001) 1827–1836.

[44] J.A. Lenis, L.J. Toro, F.J. Bolívar, Surface & Coatings Technology Multi-layer bactericidal silver - calcium phosphate coatings obtained by RF magnetron sputtering, Surf. Coat. Technol. 367 (2019) 203–211. doi:10.1016/j.surfcoat.2019.03.038.